The Journal of Experimental Biology 204, 2959–2973 (2001)
Printed in Great Britain © The Company of Biologists Limited 2001
JEB3394

Mechanisms of helical swimming: asymmetries in the morphology, movement and mechanics of larvae of the ascidian *Distaplia occidentalis*

Matthew J. McHenry*

Department of Integrative Biology, University of California, Berkeley, CA 94720, USA

*e-mail: mchenry@socrates.berkeley.edu

Accepted 11 June 2001

Summary

A great diversity of unicellular and invertebrate organisms swim along a helical path, but it is not well understood how asymmetries in the body shape or the movement of propulsive structures affect a swimmer's ability to perform the body rotation necessary to move helically. The present study found no significant asymmetries in the body shape of ascidian larvae (*Distaplia occidentalis*) that could operate to rotate the body during swimming. By recording the three-dimensional movement of free-swimming larvae, it was found that the tail possessed two bends, each with constant curvature along their length. As these bends traveled posteriorly, the amplitude of curvature changes was significantly greater in the concave-left direction than in the concave-right direction. In addition to this asymmetry, the tail oscillated at an oblique angle to the midline of the trunk. These asymmetries generated a yawing moment that rotated the body in the counterclockwise direction from a dorsal view, according to calculations from hydrodynamic theory. The tails of resting larvae were bent in the concave-left direction with a curvature statistically indistinguishable from the median value for tail curvature during swimming. The flexural stiffness of the tails of larvae, measured in three-point bending, may be great enough to allow the resting curvature of the tail to have an effect on the symmetry of kinematics. This work suggests that asymmetrical tail motion is an important mechanism for generating a yawing moment during swimming in ascidian larvae and that these asymmetries may be caused by the tail's bent shape. Since helical motion requires that moments also be generated in the pitching or rolling directions, other mechanisms are required to explain fully how ascidian larvae generate and control helical swimming.

Key words: swimming, morphology, larva, ascidian, Urochordata, *Distaplia occidentalis.*

Introduction

Organisms spanning great phylogenetic diversity and a wide range of body sizes swim along a helical path. Helical swimming has been observed in unicellular swimmers with cilia (e.g. *Paramecium caudatum*, *Loxodes rostrum*, Jennings, 1901) and flagella (e.g. *Tubularia crocea* spermatozoa, Miller and Brokaw, 1970; *Chlamydomonas reinhardtii*, Boscov and Feinleib, 1979). Many marine invertebrate larvae use cilia to swim helically (e.g. chordate lancelet larvae, Stokes, 1997; sponge planula, Bergquist et al., 1970; mollusc veligers, Jonsson et al., 1991; echinoderm doliolaria, Mladenov and Chia, 1983), and ascidian larvae follow a helical path by propelling themselves by tail undulation (Grave, 1920). Helical swimming also occurs in vertebrates that swim by undulating their bodies but have undeveloped or impaired spatial orientation. For example, early-stage larvae of the frog *Xenopus laevis* are thought to swim helically because they have undeveloped vestibular organs, and late-stage larvae can be made to swim helically by ablating their vestibular organ (Roberts et al., 2000). Ullén et al. (Ullén et al., 1995) caused adult lamprey *Lampetra fluviatilis* to swim helically by ablating their vestibular organ, thereby demonstrating that at least some vertebrates swim helically when they lack the sensory feedback necessary to control body rotation.

To move along a curvilinear trajectory such as a helix, an organism must rotate its body as it moves forward (see Crenshaw et al., 2000). An organism's weight, buoyancy and swimming hydrodynamics have all been hypothesized to generate the moments (i.e. torques) for rotation and the forces for forward movement (Young, 1995). Moments can be generated by hydrodynamics from asymmetries either in the body shape of swimmers or in the motion of their propulsive structures. Such mechanisms appear to play a role in the helical swimming of *Tubularia crocea* spermatozoa, which beat their flagella with asymmetrical undulations (Miller and Brokaw, 1970). Jennings (Jennings, 1901) suggested that helical swimming in many microorganisms is generated by asymmetrical body shapes. Knight-Jones (Knight-Jones, 1954) implied a hydrodynamic mechanism for body rotation when he reported that metachronal waves in ciliary beating are directed at an oblique angle to the long axis of the body in a diversity

of metazoans that swim helically. Although these studies suggest a variety of mechanisms for helical swimming, two fundamental questions remain untested: (i) do morphological and kinematic asymmetries generate moments that act to rotate the body during helical swimming, and (ii) how are kinematic asymmetries generated?

The present study addresses these questions by testing hypotheses about the mechanics of helical swimming in ascidian larvae. Swimming plays a brief but important role in the ecology of this relatively large group of urochordates (ascidians include around 3000 species; Jeffery, 1997). Larvae disperse in the ocean for a duration ranging from a few minutes (e.g. *Botrylloides* sp., Worcester, 1994) to 10 days (e.g. *Ascidia mentula*, Svane, 1984) and do not feed. After this dispersal phase, larvae metamorphose into a sessile juvenile form. Therefore, helical swimming in the larval phase is the only opportunity for locomotion in the life cycle of an individual.

Both morphological and kinematic asymmetries have been hypothesized to enable ascidian larvae to swim along a helical trajectory. Grave (Grave, 1920) suggested that the subtle depression on the left side of the trunk of *Aplidium constellatum* larvae contributes to the generation of their right-handed (i.e. clockwise when viewed from the rear) helical trajectory. The tail fin of *Aplidium constellaum* is thought to twist during swimming undulations and thereby cause the body to rotate (Mast, 1921). The tail of many species has been observed to bend to one side of the body when at rest (Berrill, 1950). If the flexural stiffness of the larval tail is substantial, then this asymmetry in shape could cause an asymmetry in motion that may help to rotate the body. Furthermore, if the tail stiffness resists tail bending more in one direction than the other, then further kinematic asymmetry should result.

Ascidian larvae are well suited for this investigation because their tail motion when freely swimming is easier to observe than the patterns of movement by the fields of cilia used by many other helical swimmers (e.g. bivalve veligers, Jonsson et al., 1991; ciliated metazoans, Knight-Jones, 1954; microorganisms, Jennings, 1901). The study species, *Distaplia occidentalis*, is abundant in Northern California, USA, and is reproductively active for a long period during the summer and autumn. The larvae of *Distaplia occidentali*s possess a visibly dark ocellus and a light trunk, which makes it possible to measure the body orientation in three dimensions from video sequences. Furthermore, larvae of *D. occidentalis* are relatively large (mean body length 3.50 mm), so tail stiffness could be measured more easily than in smaller larvae.

By measuring the body shape of resting larvae, the flexural stiffness of the tail and the motion of the body during swimming, I tested the following hypotheses: (i) that the trunk and tail fin possess morphological asymmetries; (ii) that the tail undulates with an asymmetrical kinematic pattern; (iii) that the flexural stiffness provides greater resistance to deflection in one direction than the other; and (iv) that kinematic asymmetries generate moments that act to rotate the body.

Materials and methods

In the months of August and September in 1999, *Distaplia occidentali*s (Bancroft) were collected from floating docks at the Spud Point Marina in Bodega Bay, CA, USA, in water that was between 11 and 16 °C. Colonies were transported within 2 h to a cold room at the University of California, Berkeley, CA, USA, where they were held at temperatures between 13 and 17 °C. To stimulate release of larvae, colonies were exposed to bright artificial light after being kept in darkness overnight (Cloney, 1987). Released larvae were placed in an aquarium that was cooled with a water bath at 15 °C. Within 2 h of release, one of three experiments was conducted on an individual larva. A larva was (i) videotaped while swimming, (ii) photographed while resting or (iii) used for measurements of tail flexural stiffness. All experiments were conducted within 4 days of collection of the adult colony.

Morphometrics

Digital still images of resting larvae from dorsal and lateral views were captured by computer (7100/80 PowerPC Macintosh with Rasterops 24XLTV frame grabber) using a video camera (Sony, DXC-151A) mounted on a dissecting microscope (Nikon, SMZ-10A). Images of the body shape were measured using NIH Image software (version 1.62) on an Apple Macintosh G3 computer. These images had a spatial resolution of 640×480 pixels, with each pixel representing a square with sides measuring approximately 7 μm.

All morphometric measurements were made relative to the body's midline. In the trunk, this midline was defined as the axis running through the center of intersection of the trunk with the tail and the center of the three adhesive papillae at the anterior end of the trunk (Fig. 1). To test for dorso-ventral morphological asymmetries, the distance between the dorsal margin of the trunk and the midline was compared with the distance between the ventral margin and the midline at 20 equally spaced longitudinal positions. At each of these trunk positions, the distance between the right margin of the trunk and the midline was compared with the distance between the left margin and the midline as a measure of bilateral symmetry (Fig. 2).

The larval tail is composed of a cellular portion, containing the notochord, muscle and nerve cells, and the extracellular tail fin made of tunic tissue (Burighel and Cloney, 1997). The midline of the tail at each longitudinal position was centered between the left, right, dorsal and ventral margins of the cellular region. To test for dorso-ventral asymmetries in the tail fin, the distance from the midline to the dorsal margin was compared with the distance from the midline to the ventral margin at 10 equally spaced longitudinal positions.

The curvature of the tail of resting larvae was measured to determine whether larvae are consistently bent towards the same side of the body. Resting curvature was measured as the mean value of discrete measures of curvature (see Fig. 1B) at all tail positions. The present study considers the side of the tail with the nerve cord to be in the dorsal direction (as in Burighel and Cloney, 1997) for the trunk and tail (this is not

always the convention for ascidian larvae; e.g. Cavey and Cloney, 1972).

Kinematics

Swimming larvae were filmed simultaneously with two digital high-speed video cameras recording at 500 frames s^{-1} (Redlake PCI Mono/100S Motionscope, 320×280 pixels per camera, each equipped with a 50 mm macro lens (in the arrangement described by Crenshaw, 1991). The cameras were directed in perpendicular directions and both were focused on a small volume (1 cm^3) of water in the center of an aquarium (3 cm×3 cm×6 cm). Larvae were illuminated from the side with two fiber-optic lamps (Cole Parmer 9741-50). The aquarium was built with a separate outer chamber into which chilled water flowed from a water bath equipped with a thermostat (VWR Scientific, 1166) to maintain a water temperature of approximately 15 °C. Larvae generally swam in the vertical direction and passively sank to the bottom of the tank when resting. As in most species of ascidian larvae, swimming could be stimulated by briefly dimming the illuminators (the 'shadow response'; Grave, 1941). Once initiated, swimming behavior continued with the lights on and ceased after larvae arrived at the water's surface.

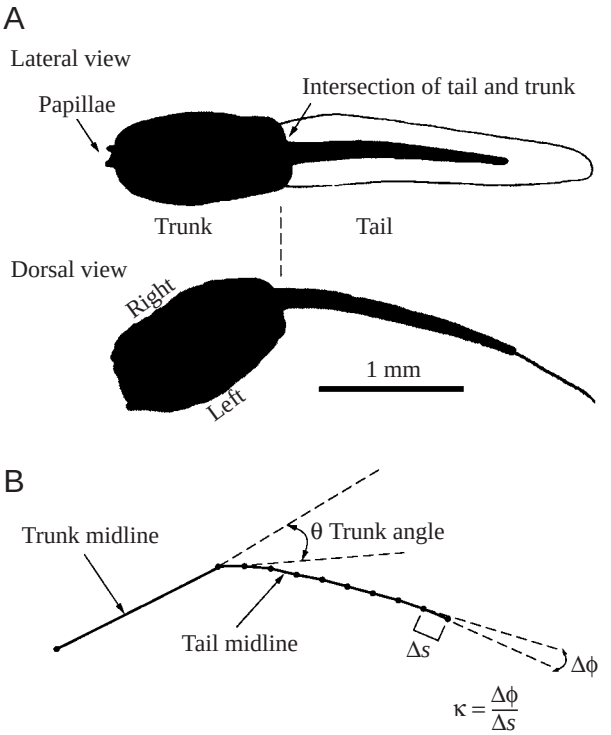

Fig. 1. Typical shape of the resting larval body. (A) Silhouettes of lateral and dorsal views of a larva, traced from video images. The tail fin is shown in white. The concave-left bend in the tail of this individual can be seen from the dorsal view. (B) The midline measured from the dorsal view of the same individual. Trunk angle (θ) is the angle between the trunk's midline and the first anterior segment of the tail. Curvature for a tail segment (κ) is equal to the angular flexion, Δϕ, between the neighboring segments, divided by the length of the segment, Δs (Thomas and Finney, 1980).

The three-dimensional swimming movements of the trunk and tail were acquired and analyzed with custom-designed computer programs. Since the trunk was assumed to be rigid, its motion was described by changes in the position of a point in the center of the three anterior papillae and a second point at the intersection of the trunk and tail (Fig. 1B). The coordinates of both points were manually selected with an Apple PowerMac G3 with NIH Image software (version 1.62). Using the same procedure, the movement of the ocellus was tracked to later reconstruct the body axes in the analysis stage. Since larvae were the brightest figures (i.e. the pixels with the lowest values) in the video frames, the silhouette of the tail could be traced automatically. The midline of the tail was found by 'dissolving' its silhouette (see Russ, 1999) to a line with a width of 1 pixel with a custom-designed macro in NIH Image. A second macro found between 5 and 20 coordinate pairs (*X* and *Z*) along the midline's length in one video frame, then referred to the corresponding video frame recorded by the other camera to find matching coordinates in the third dimension (*Y*). This acquisition of three-dimensional coordinates was completed for every frame of video for a period of approximately 1 s (500 video frames) in sequences in which larvae appeared to swim vertically along a straight helical trajectory.

The tail kinematics were analyzed in four stages: (i) the coordinates of unequal number and spacing in the camera's frame of reference were transformed into 20 evenly spaced points in the frame of reference of the body, (ii) the shape of the midline of the tail was described using the angle between the trunk and the tail (trunk angle) and a curvature function for each instant of time, (iii) changes in tail midline shape and trunk angle with time were described and (iv) asymmetries in this kinematic pattern were tested. These four stages are described below in detail.

Stage 1: transforming midline coordinates into evenly spaced points in the body's frame of reference

The first stage in the kinematic analysis transformed the variable number of coordinates describing the tail midline (described above) into 20 evenly spaced points for each instant of time. Programs for this analysis were written with Matlab software (version 5.2, Mathworks). The positions of points along the length of the tail were calculated by measuring the sum of the distances between points. To describe the relationships between tail position and each of the three spatial dimensions with a continuous expression, coefficients describing a fifth-order polynomial were found by least-squares approximation for each spatial dimension. Polynomials of the fifth order were the lowest order that described the shape of the tail well. Equidistant coordinate points were found by solving these functions for 20 tail positions at equal intervals. The result was a description of 19 tail segments of equal length in three-dimensional space. To ensure against operator error and smoothing errors, two-dimensional projections of these coordinates were plotted back on the original video frames for verification. Swimming

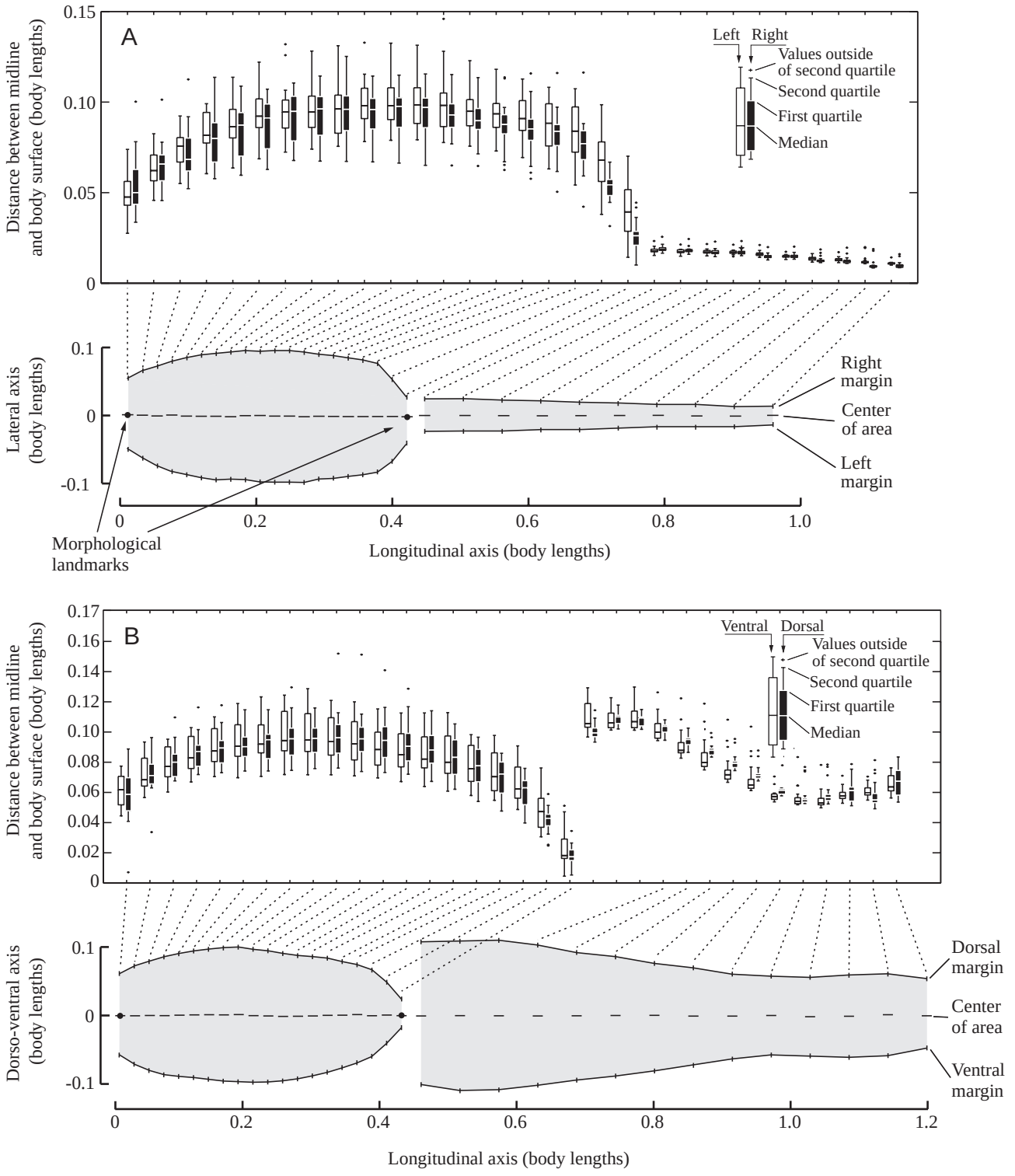

Fig. 2. The symmetry of larval tails and trunks. All measurements are relative to the midline axis and are expressed in terms of body length (see Materials and methods). The lower plots in A and B give the mean values for the surface of the trunk and tail (vertical dashes). Dotted lines connect body positions along the longitudinal axis from the lower image with their corresponding position in the box plot data shown above. The upper plots show the median and quartiles of data on opposite sides of the midline (N=18). (A) In the lower graph, the average shape of the larval body from a dorsal view is traced with vertical tick marks. The thickness of the cellular portion of the tail is visible in the tail region. The distance between the midline and the left margin is statistically indistinguishable from the distance between the midline and the right margin at all antero-posterior positions. (B) In the lower graph, the shape of the average larva as viewed from a lateral perspective is traced with vertical tick marks. In the tail region, the profile of the tail fin is traced. No significant differences were found between the distances of the dorsal (filled columns) and ventral (open columns) margins from the midline at any position along the length of the body.

sequences were discarded if coordinate points were not aligned with the midline of the body. This criterion combined with the relatively brief duration that individuals remained within view of both cameras restricted the analysis to a single tail-beat cycle per individual.

Using methodology described by Craig (Craig, 1989), the body's frame of reference was defined for larvae using the three coordinate points describing the trunk's position. The origin of the body's coordinate system was defined as the intersection point between the tail and trunk, and the anterio-posterior axis was defined by the line between this point and the center of the papillae at the anterior end of the trunk. Using the position of the ocellus within the trunk measured in resting individuals, the lateral and dorso-ventral axes were reconstructed. Tail coordinates in the camera's frame of reference were then transformed into coordinates relative to the body's frame of reference.

Stage 2: describing tail midline shape

By observing the swimming of ascidian larvae, it was apparent that conventional methods for kinematic description would not suffice. The classical kinematic analyses for fish swimming (e.g. Lighthill, 1975; Webb et al., 1984) were insufficient because (i) no simple axis of progression (e.g. the straight path of a swimming fish; McHenry et al., 1995) exists for swimmers following a three-dimensional curvilinear trajectory, (ii) the curvature of the tail was so great that it could not be described by a function with a single independent variable in Cartesian space and (iii) symmetrical kinematics could not be assumed. Therefore, coordinates describing tail shape in single video frames were described by the angle between the trunk and the tail (trunk angle) and curvature (κ) as a function of tail position. For these measurements, the discrete form of curvature was used (see Fig. 1B).

Brokaw (Brokaw, 1965) found that the shape of the flagellum of bull spermatozoa during swimming was better described by a series of adjoining semi-circles than by conventional kinematic equations (e.g. Gray and Hancock, 1955). As is characteristic of circles, these semi-circular portions of the tail were constant in curvature along their length. The tail shape of *D. occidentalis* may also be described by bends of constant curvature, one bent to the right and another bent to the left of the body (Fig. 3A,C,E). Therefore, tail shape at a single instant of time may be described by one concave-left curvature (κ_{CL}), one concave-right curvature (κ_{CR}) and the position along the body's length (s) where the semi-circles intersect, which is the inflection point (s_i). The following equation shows how curvature varies as a function of tail position:

$$\kappa(s,t) = \begin{cases} \kappa_{CR} \text{ for } (s<s_i \text{ and } t<\frac{1}{2}) \text{ or } (s>s_i \text{ and } t>\frac{1}{2}) \\ \kappa_{CL} \text{ for } (s>s_i \text{ and } t<\frac{1}{2}) \text{ or } (s<s_i \text{ and } t>\frac{1}{2}) \end{cases} . \quad (1)$$

This expression means that, in the first half of a tail beat (t<0.5), tail curvature, $\kappa(s,t)$, anterior to the inflection point (s<s_i) is equal to κ_{CR}, but is equal to κ_{CL} posterior to the inflection point (s>s_i). In the second half of the tail beat (t>0.5), tail curvature equals κ_{CL} anterior to (s<s_i) and κ_{CR} posterior to (s>s_i) the inflection point. This pattern of curvature is illustrated for two instants of time in Fig. 3, in which concave-right curvatures are positive in sign and concave-left curvatures are negative. Trunk angle (θ), a variable that completed the description of body shape, is the angle between the trunk's midline and the first anterior segment of the tail (Fig. 1B).

The following equations were used to translate the midline shape variables (θ, κ_{CL}, κ_{CR} and s_i) into a series of coordinate points that could be compared with the data:

$$x_n = \Delta s \cos\theta + \sum_{i=2}^{n} \Delta s \cos[\Delta s \kappa(s_i)] , \quad (2)$$

$$y_n = \Delta s \sin\theta + \sum_{i=2}^{n} \Delta s \sin[\Delta s \kappa(s_i)] , \quad (3)$$

where Δs is tail segment length and n is the tail segment number. These equations calculate the position of the posterior end of segment n. These relationships show that the position of the end of the first tail segment (n=1) is dependent on the trunk angle θ. The curvature at the intersection of each segment pair (s_n) affects the position of all segments posterior to it. By trial and error, values for θ, then anterior curvature (κ_{CL} or κ_{CR}), then the inflection point (s_i) and then posterior curvature (κ_{CL} or κ_{CR}) were selected on the basis of the visual closeness of fit between the curve that they described and the data. Fig. 3 illustrates the midline data and the curves that describe their shape.

Stage 3: measuring shape changes over time

After determining values for the midline shape variables (θ, κ_{CL}, κ_{CR} and s_i) for each instant in time at 2 ms intervals, the next objective was to describe how these variables changed with time. An equation describing how each variable changed with time was created (see Results), and the values for parameters in these equations were found using a non-linear least-squares algorithm (Matlab version 5.2, Mathworks). Although the exact form of these equations could not be predicted, their parameters were apparent from qualitative observation of the swimming motion. The inflection point s_i was expected to travel down the tail at some wave speed ε. Trunk angle θ appeared to vary periodically with time and was therefore expected to oscillate above and below a value β with an amplitude equal to α_θ. Since tail curvature has been shown to oscillate with time in swimming fish (e.g. Katz and Shadwick, 1998), it was expected that the amplitude of changes in concave-left curvature (α_{CL}) and concave-right curvature (α_{CR}) could be measured.

Stage 4: testing for kinematic asymmetries

Asymmetries in undulatory motion were described by how

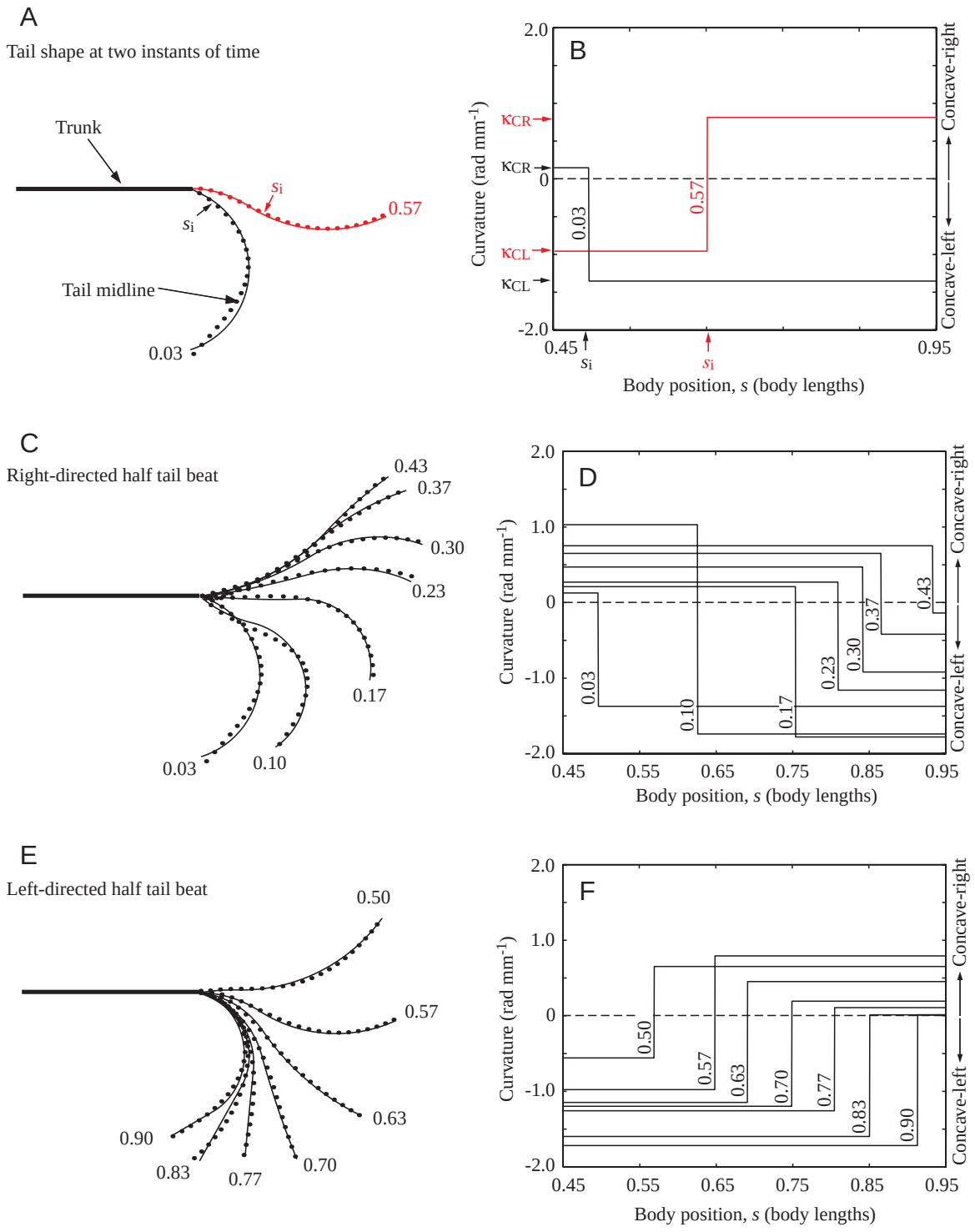

Fig. 3. Typical changes in tail midline shape during a tail beat illustrated by one individual. On the left are coordinates for the midline taken from a dorsal view and the curves that approximate their shape. The numbers at the end of the curves specify the corresponding time (t) in terms of the tail-beat cycle. The curvature profiles corresponding to these curves are shown on the right. (A,B) t=0.03 tail-beat cycles (shown in black), is within the first half of the tail beat (t<0.5) and tail motion is directed towards the right side of the body. At this moment, the section of the tail anterior to the inflection point (s<s_i) bends concave-right with a curvature equal to κ_{CR}, and positions posterior to the inflection point (s>s_i) are bent concave-left with a curvature of κ_{CL}. t=0.57 tail-beat cycles (shown in red) is within the second half of the tail beat (t>0.5), and the tail is moving towards the left side of the body. Tail curvature is equal to κ_{CL} anterior to the inflection point (s<s_i) and to κ_{CR} posterior to the inflection point (s>s_i). (C,D) Tail motion shown at 4 ms intervals (roughly 0.03 tail-beat cycles) for the first half of a tail beat (t<0.5), when the tail is moving towards the right side of the body. Note that the magnitude of curvature in both directions (κ_{CL} and κ_{CR}) changes with time. (E,F) The motion during the left-directed, second half of the tail beat (t>0.5) shown at 4 ms intervals. Again, curvature in both directions varies with time.

each of the variables describing midline shape (θ, κ_{CL}, κ_{CR} and s_i) changed with time. Three sources of asymmetry were hypothesized and tested (see below). (i) As observed in the turning maneuvers of the eel *Anguilla rostrata* (Gray, 1933), the speed with which waves travel down the tail may vary with time. Wave speed ε was hypothesized to be different between the first and second halves of the tail-beat cycle. (ii) An asymmetry would also result if the trunk angle oscillated around a non-zero baseline value (β). (iii) Unequal values for the amplitude of curvature changes between the concave-left (α_{CL}) and concave-right (α_{CR}) sides should also cause asymmetry.

Tail bending stiffness

To address whether tails resist deflection more in one direction than the other, three-point bending tests were conducted using the general approach taken by Adams et al. (Adams et al., 1990) for *Xenopus laevis* embryonic notochords. A beam of known stiffness was pushed against the lateral surface of the tail to place it in bending. This beam, which was composed of silver, was 5 cm in length and 100 μm in diameter. The two static points held in opposition to the beam were placed 0.4 mm apart. All lateral deflections of both the silver beam and the portion of tail in bending were kept below 10 % of their length in order not to violate the assumptions of low-deflection beam theory. This theory uses the following equation to calculate flexural stiffness from a three-point bending test (Adams et al., 1990):

$$EI = \frac{Fl^3}{48\delta}\,, \tag{4}$$

where EI is the flexural stiffness, F is the force that the tip of the silver beam exerted on the tail, l is the length of the portion of the tail between the two supports and δ is the lateral deflection of the tail resulting from the load.

Hydrodynamic model

Kinematics and morphometrics alone can only provide qualitative hypotheses for their effect on the mechanics of swimming. The hydrodynamic model of Jordan (Jordan, 1992) was used to calculate a quantitative prediction of the turning moments generated by the kinematics and morphometrics measured for *D. occidentalis*. This model is appropriate for the size and swimming speed range of ascidian larvae, where both viscous and inertial forces are important to their hydrodynamics. Reynolds number (*Re*) represents the ratio of inertial to viscous forces and it is calculated as:

$$Re = \frac{UL}{\nu}\,, \tag{5}$$

where U is the swimming speed, L is a characteristic length (taken as the distance between the anterior margin of the trunk and the posterior margin of the tail) and ν is the kinematic viscosity. The mean ±1 S.D. *Re* calculated for *D. occidentalis* larvae was 92.9±20 (N=11; see Table 1).

Jordan (Jordan, 1992) modeled the hydrodynamic forces generated by swimming at intermediate Reynolds' numbers ($1<Re<1000$) by body undulation for the chaetognath *Sagitta elegans*. According to this blade-element model, the force acting on a segment of the tail is the vector sum of the acceleration reaction (i.e. 'reactive forces', $F_{reactive}$), and the quasi-steady forces acting normal and tangential to the segment (i.e. 'resistive forces', $F_{resistive}$). The following equations were used to calculate the instantaneous force (F_{total}) acting on a tail segment:

$$F_{total} = F_{resistive} + F_{reactive}\,, \tag{6}$$

$$F_{resistive} = \tfrac{1}{2}\rho A(C_n V_n^2 \hat{\mathbf{n}} + C_t V_t^2 \hat{\mathbf{t}})\,, \tag{7}$$

$$F_{reactive} = \frac{\Delta V_n}{\Delta t}\, m\hat{\mathbf{n}}\,, \tag{8}$$

where ρ is the density of water, A is the surface area of the tail segment, C_n and C_t are the respective normal and tangential force coefficients, V_n and V_t are the normal and tangential components of velocity for the segment, $\hat{\mathbf{n}}$ is the unit vector normal to the surface of the tail segment, $\hat{\mathbf{t}}$ is the unit vector tangential to the surface of the tail segment and m is the mass of water accelerated by the tail segment, known as the added mass. A unit vector has a magnitude of 1 and, in this case, points in the normal or tangential direction of a tail segment with respect to the global (i.e. inertial) frame of reference (Thomas and Finney, 1980). Added mass was calculated using the method described by Lighthill (Lighthill, 1975) for each tail segment:

$$m = \tfrac{1}{4}\pi\rho h^2 \Delta s\,, \tag{9}$$

where Δs is the length and h is the height of the tail segment (the distance between the dorsal and ventral margins of the fin). Acceleration of a tail segment was calculated as the component of the discrete changes in velocity in the direction normal to the tail's surface (ΔV_n) divided by change in time (Δt). The following equations for the normal and tangential force coefficients were used (Jordan, 1992):

$$C_n = 10^{[1.28-0.809(\log Re)+0.134(\log Re)^2]}\,, \tag{10}$$

$$C_t = 0.64(Re)^{-1/2}\,. \tag{11}$$

Since larvae swam steadily, the conventional measure of *Re* for undulatory swimmers (equation 5) was used instead of the method of Jordan (Jordan, 1992), which calculates *Re* for each instant of time.

The forces and moments generated by each tail segment were calculated using the measured morphometrics of the tail (see above) and the kinematics from the body's frame of reference (see above) for each instant of time. The origin of this coordinate system was positioned at the intersection of the tail and the trunk, a point I will refer to as the center of body. The total moment around the center of body was equal to the sum of all moments generated by tail segments. To assess whether the kinematics generated greater moments in one direction than the other, the mean value of total moments during left-directed half tail beats was compared with the mean

value during right-directed half tail beats. These calculations were executed with Matlab (version 5.2, Mathworks) software running on a computer (IBM Thinkpad 760XD).

Statistical design

Statistical tests were used to detect asymmetries in body morphology, kinematics, turning moments and the bending stiffness of the tail. A Kolomogorov–Smirnov test was used to test the normality of data (Sokal and Rohlf, 1995). When samples were found not to be normally distributed (i.e. Kolomogorov–Smirnov test, $P<0.05$), the median and range were reported. The assumption of normality was avoided when comparing samples by using a non-parametric Mann–Whitney *U*-test. Samples were considered significantly different if the Mann–Whitney *U*-test found $P<0.05$ (Sokal and Rohlf, 1995). Normally distributed samples (i.e. Kolomogorov–Smirnov test, $P>0.05$) were reported by their mean and standard deviation. These distributions were considered significantly different if a Student's *t*-test found $P<0.05$. Since no data could be assumed to have a normal distribution, data are illustrated in the figures by their median, range, quartiles and outliers rather than by their mean and standard deviation.

Results

Symmetry of the trunk and tail fin

In the trunk, no significant differences were detected between the distances from the left margin of the body to the midline and from the right margin to the midline (Mann–Whitney *U*-test, $P>0.05$, $N=18$; Fig. 2A). Comparisons between the distances from the midline to the dorsal margin of the larva and the distances from the midline to the ventral margin were also not significantly different at any position along the length of the trunk or tail (Mann–Whitney *U*-test, $P>0.05$, $N=18$; Fig. 2B). These data suggest that the bodies of larvae are symmetrical with respect to the midline in all individuals ($N=18$). Although symmetrical, the tails of all larvae were bent in the concave-left direction, as illustrated by the individual shown in Fig. 1 (measurements of resting tail curvature given below).

Symmetry of the undulatory motion

An example of the changes with time in the shape of the midline of the tail in a swimming larva is illustrated in Fig. 3. Changes in concave-left curvature (κ_{CL}), concave-right curvature (κ_{CR}), the position of the inflection point (s_i) and the trunk angle (θ) were described by the following functions of time (Fig. 4):

$$s_i(t) = \varepsilon t\,, \tag{12}$$

$$\kappa_{CL}(t) = -\alpha_{CL}[\cos(2\pi t) + 1]\,, \tag{13}$$

$$\kappa_{CR}(t) = \alpha_{CR}\{\cos[2\pi(t + \tfrac{1}{2})] + 1\}\,, \tag{14}$$

$$\theta(t) = \alpha_{\theta}\cos(2\pi t) + \beta\,. \tag{15}$$

The data used to test the three possible sources of kinematic asymmetry are shown in Fig. 5. The amplitude of concave-left curvature (median 0.68 rad mm^{-1}, range 0.41 rad mm^{-1}, $N=11$) is significantly different (Mann–Whitney *U*-test, $P\ll0.001$, $N=11$; Fig. 5A) from concave-right curvature in the same tail beat (median 0.42 rad mm^{-1}, range 0.40 rad mm^{-1}, $N=11$), and this difference generates asymmetry in the motion of the tail. The ratio of α_{CL} to α_{CR} is a measure of kinematic asymmetry; a value of 1 corresponds to no asymmetry due to curvature differences. Because it is often more convenient to measure maximum values of curvature than the amplitude of curvature changes, the ratio of α_{CL} to α_{CR} for swimming sequences was compared with the ratio of maximum curvature in the concave-left (κ_{CLmax}) and the concave-right (κ_{CRmax}) directions for the same sequences. These ratios were found to be statistically indistinguishable (unpaired two-tailed *t*-test, $P=0.624$), as represented by the following relationship:

$$\frac{\alpha_{CL}}{\alpha_{CR}} \approx \frac{\kappa_{CLmax}}{\kappa_{CRmax}}\,. \tag{16}$$

The ratio α_{CL} to α_{CR} (1.9±0.8, mean ±1 S.D., $N=11$) was greater than 1 in all larvae (Kolomogorov–Smirnov, $P>0.05$), which means that the maximum curvature on the concave-left side was greater than the curvature on the concave-right side. Trunk angle oscillated around a baseline value (β) that was significantly less than zero (Fig. 5C) (Kolomogorov–Smirnov, $P>0.05$; mean ±1 S.D. –0.13±0.08 rad; one-tailed *t*-test, $P<0.001$, $N=11$), meaning that the trunk is generally bent in the concave-left direction. Wave speed (ε), in contrast, did not appear to be a source of kinematic asymmetry because it was not significantly different between the left-directed (median 8.3 mm s^{-1}, range 47.5 mm s^{-1}, $N=11$) and right-directed (median 42.2 mm s^{-1}, range 37.5 mm s^{-1}, $N=11$) halves of the tail beat and therefore cannot cause any asymmetries (Mann–Whitney *U*-test, $P=0.49$, $N=11$; Fig. 5B).

To summarize these results, the tails of larvae moved with asymmetries that resulted in the tail bending more towards to the left than towards the right (Fig. 3, Fig. 4, Fig. 5). Two parameters describe these asymmetries: curvature amplitude and baseline trunk angle. Curvature amplitude was greater in the concave-left than in the concave-right direction. Baseline trunk angle was found to be significantly less than zero, which means that the tail oscillated at an oblique angle towards the left of the midline of the trunk.

The median tail curvature measured over the tail-beat cycle was compared with the tail curvature of resting larvae. The median value was chosen because, unlike the mean, its value does not vary with the speed of tail motion. There was no significant difference between the tail curvature of resting larvae and the median value for tail curvature in swimming larvae (both samples normally distributed: Kolomogorov–Smirnov test, $P>0.05$; two-tailed, unpaired *t*-test, $P=0.964$, $N=11$; Fig. 6C).

Flexural stiffness of the tail

Larval tail bending stiffness did not require more force to deflect the tail in one direction than in the other (Fig. 7). This result refutes the hypothesis that an asymmetry in flexural

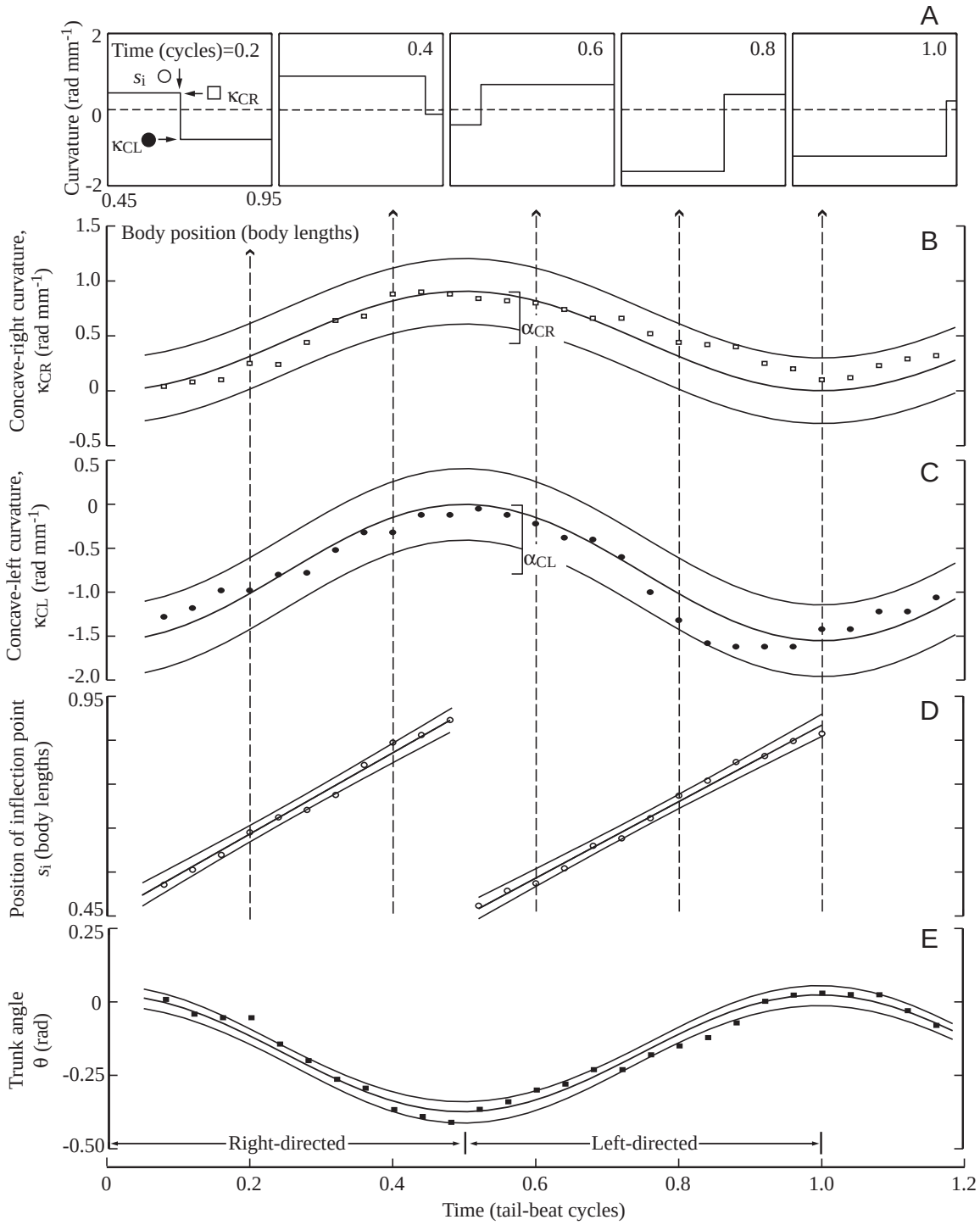

Fig. 4. Kinematic variables as a function of time. Body movement for 1.2 tail beats is shown for one individual moving with the typical pattern observed during steady swimming. Thick lines show trends found by least-squares curve-fitting and thin lines denote 95 % confidence intervals (calculated by Matlab version 5.2, Mathworks). See Results for the functions fitted to these data. Negative values for curvature are directed concave-left and positive values are concave-right. (A) Graphs of curvature as a function of body position at five different instants separated by intervals of 0.2 tail-beat cycles. The values at each instant for concave-right curvature (κ_{CR}), concave-left curvature (κ_{CL}) and the position of the inflection point (s_i) define the shape of this step function. (B,C) Variation in κ_{CR} (B) and κ_{CL} (C). Note that the amplitude of changes in concave-right curvature (κ_{CR}) is smaller than the amplitude of concave-left curvature changes (κ_{CL}). Oscillations in κ_{CR} are of opposite sign and are half a tail beat out of phase with the changes in κ_{CR}. (D) Variation in the inflection point in curvature (s_i) with time demonstrates a linear propagation of the inflection point down the length of the tail. (E) The angle between the trunk's midline and the first anterior tail segment (see Fig. 1) with time in phase with κ_{CR}.

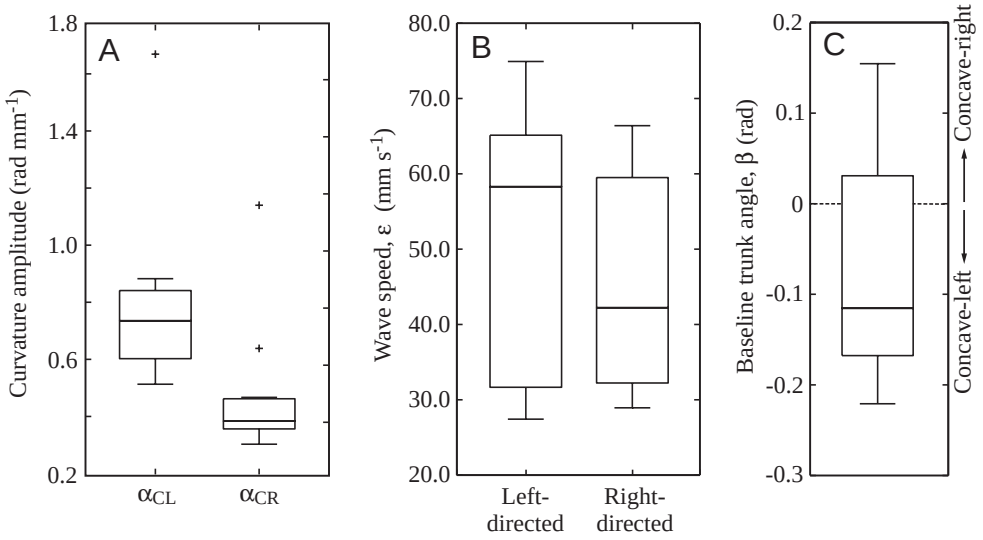

Fig. 5. Possible sources of kinematic asymmetry. (A) Differences between concave-left (α_{CL}) and concave-right (α_{CR}) curvature amplitude, (B) differences in wave speed (ε) between left-directed and right-directed half tail beats, and (C) non-zero baseline trunk angles (β), N=11. All were hypothesized to generate kinematic asymmetries (see Materials and methods), but asymmetries were measured only in the differences in curvature amplitude (A) and the non-zero values for baseline trunk angle (C). As in Fig. 2, the middle line in each box plot represents the median, the top and bottom edges of the box show the first quartile, error bars denote the second quartile and plus signs indicate values outside the second quartile.

stiffness causes the kinematic asymmetries observed. Although stiffness in some individuals was greater in the concave-left direction than the concave-right direction (e.g. Fig. 7A), concave-left stiffness (median 0.29×10^{-13} N m^2, range 2.01×10^{-13} N m^2, N=13) was generally not significantly different (Mann–Whitney U-test, P=0.419, N=13) from concave-right stiffness (median 0.40×10^{-13} N m^2, range 1.08×10^{-13} N m^2, N=13; Fig. 7B) among larvae.

Turning moments predicted from the kinematic asymmetries

The hydrodynamic model of Jordan (Jordan, 1992) for intermediate-*Re* swimming was used to formulate predictions for the turning moments generated by the kinematic patterns observed for *D. occidentalis* larvae (Fig. 8). The time-averaged mean moment ($1.75\times10^{-9}\pm0.12\times10^{-9}$ N m, mean ±1 S.D., N=11) for the kinematics of single tail beats was significantly greater than zero and therefore acted in the counterclockwise direction (Kolomogorov–Smirnov test, P>0.05; one-tailed, unpaired t-test, P=0.019). This result supports the hypothesis that the kinematic asymmetries observed (Fig. 3, Fig. 4, Fig. 5) act as a mechanism to rotate the body.

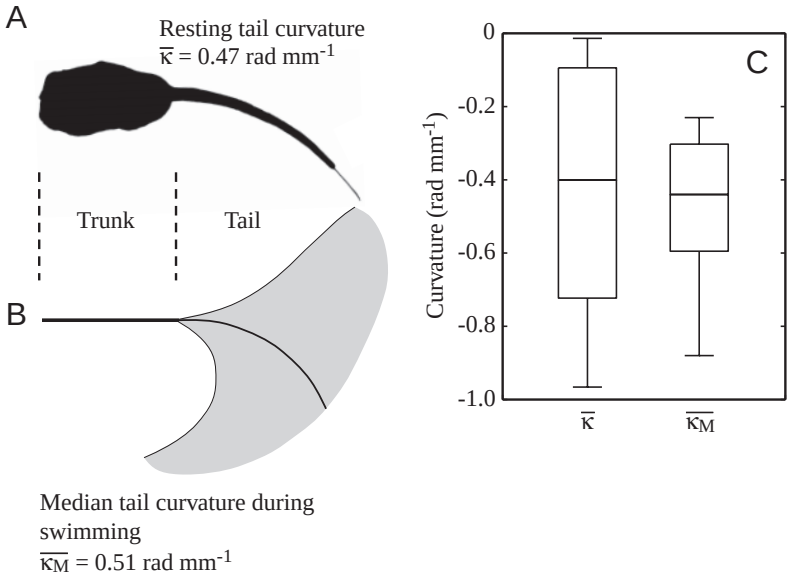

Fig. 6. Resting tail curvature compared with tail curvature during swimming. $\overline{\kappa}$ is the mean tail curvature over the length of the tail. (A) Silhouette of a resting individual from a dorsal view with a mean tail curvature ($\overline{\kappa}$) of 0.47 rad mm^{-1}. (B) A midline for the individual shown in A is drawn with a tail curvature equal to the median value for tail curvature $\overline{\kappa_M}$ measured during swimming ($\overline{\kappa_M}$=0.51 rad mm^{-1}). The range of tail excursion during swimming is shown in gray. (C) Comparison of the tail curvatures of resting larvae with the median tail curvatures of an independent sample of swimming larvae shows the statistically indistinguishable differences in curvature between samples (N=11). The middle line in the box plot represents the median, the top and bottom edges of the box show the first quartile and error bars denote the second quartile.

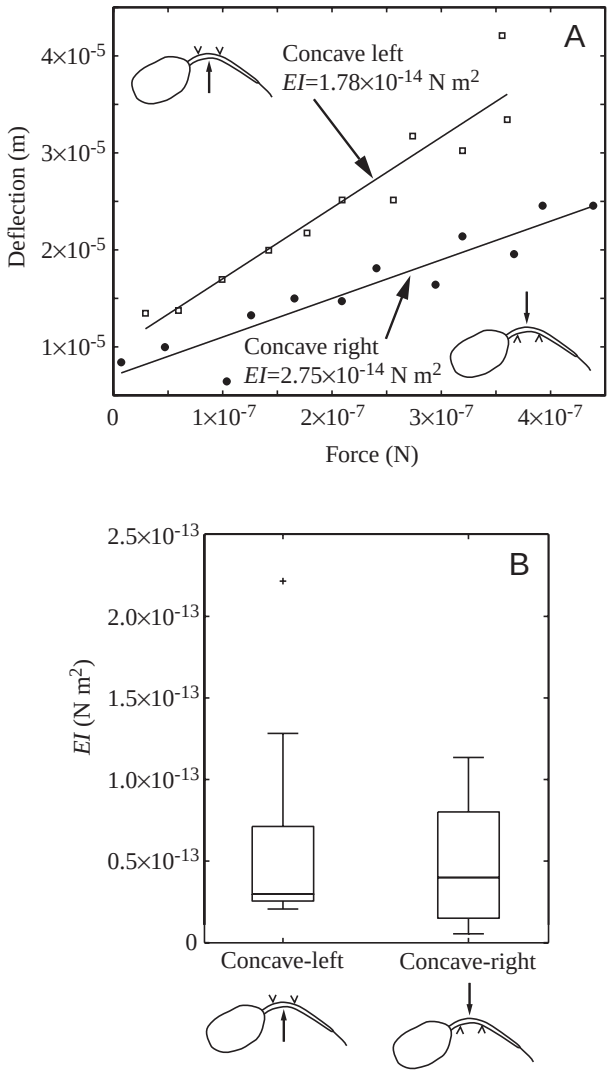

Fig. 7. Flexural stiffness *EI* of the tail in the two lateral directions compared. (A) Representative data for one individual showing the linear changes in tail deflection that result when forces between 0.1×10^{-7} and 4.5×10^{-7} N are applied laterally. The calculations for *EI* (see Materials and methods) derived from the least-squares slopes suggest that bending stiffness is greater in the concave-right direction than in the concave-left direction for this individual. (B) Summary results for flexural stiffness in both directions for all individuals tested (N=13). Stiffness measured when bending in the concave-left direction was not significantly different from bending in the concave-right direction. The middle line in the box plot represents the median, the top and bottom edges of the box show the first quartile, error bars denote the second quartile and plus signs indicate values outside the second quartile.

Discussion

Generation of kinematic asymmetries

The similarity between median tail curvature during swimming and the tail curvature of larvae at rest (Fig. 6) suggests that the shape of the resting tail may affect the symmetry of tail midline kinematics. However, if the muscle stress required to bend the tail is negligible compared with the stress that the muscles are capable of generating, then it is unlikely that the resting shape of the tail affects the swimming motion. The data presented here for the flexural stiffness of the tail (Fig. 7) may be used to estimate the muscle stress required to bend the tail.

If a larva were to bend its tail by isometric contraction of its muscles on one side, then the moment generated at any point along the tail's length should be resisted by a moment generated by the flexural stiffness of the tail. This situation is modeled in the relationship below, in which the symbols on the left represent the moment generated by the muscles and the symbols on the right represent the moment generated by the passive properties of the tail (Denny, 1988):

$$F_{\mathrm{m}}z = \kappa EI\,, \tag{17}$$

where the product of muscle force (F_{m}) and the distance (z) between the neutral axis and the muscle's center is equal and opposite to the product of the curvature of the tail (κ) and its flexural stiffness (*EI*). Since muscle force is the product of muscle stress (σ) and the cross-sectional area of the muscle (S_{m}), it follows that:

$$\sigma = \frac{\kappa EI}{S_{\mathrm{m}}z}\,, \tag{18}$$

To estimate the isometric muscle stress necessary to bend the tail, values for z (9.3×10^{-6} m) and S_{m} (3.3×10^{-11} m) were measured from the transverse section of a *D. occidentalis* tail pictured in fig. 2 of Cavey and Cloney (Cavey and Cloney, 1972). Using the absolute value of the largest value for κ_{CLmax} (2.5×10^{3} rad m^{-1}) (Table 1) and the maximum value for *EI* (2.2×10^{-13} N m^2) (Fig. 7) recorded in the present study, a high boundary of σ equals 1800 kPa. By the same calculation, using the smallest values for κ_{CRmax} (0.7×10^{3} rad m^{-1}) and *EI* (5.0×10^{-15} N m^2), a low boundary for σ equals 11 kPa. For comparison, maximum isometric stress for invertebrate muscle ranges between 100 and 1000 kPa (Daniel, 1995), but there are no published values for ascidians. These rough estimates suggest that the stress required simply to bend the tail is at least 10 % of the maximum stress that the muscle can generate. Since animals generally generate muscle stresses much lower than isometric values during steady locomotion (Full, 1997), it is likely that a much larger fraction of the total force generated by the muscles is used just to bend the tail. It is therefore plausible that the flexural stiffness measured (Fig. 7) is great enough that the resting curvature of the tail affects the symmetry of swimming kinematics.

The mechanics of helical swimming

Although the results presented here emphasize the importance of kinematic asymmetries to the hydrodynamics of swimming in *D. occidentalis* larvae, this mechanism alone is insufficient to explain the dynamics of helical swimming. If the tail fin does not twist during swimming, the asymmetry in lateral undulations described here (Fig. 5) should result in swimming along a circular, not helical, trajectory. Tail motion in the frontal plane only generates forces within that plane and

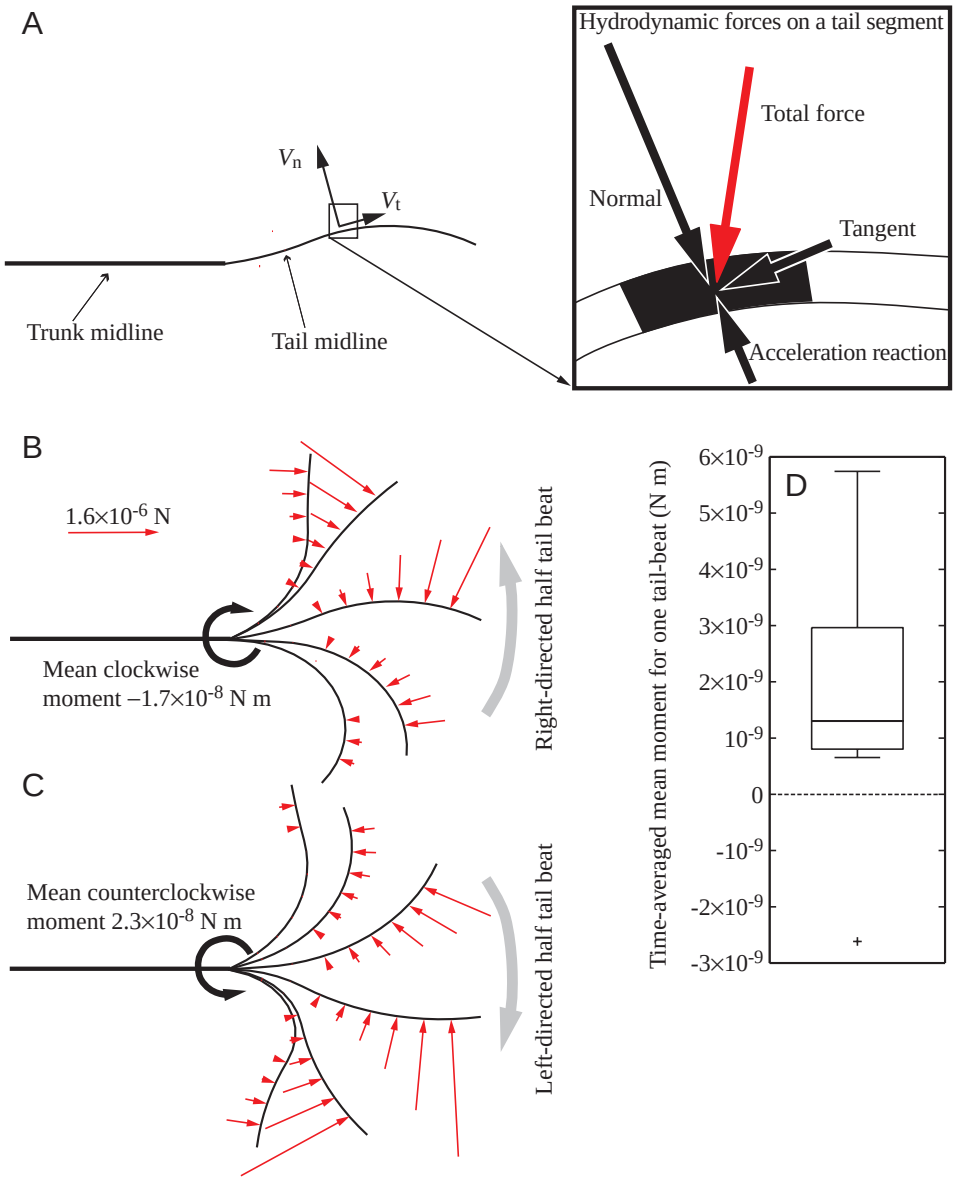

Fig. 8. Theoretical predictions for the turning moments generated by hydrodynamic forces. (A) The midline of a larval body shown from a dorsal view. At this instant, the tail is beating towards the right of the body, so the normal component of the tail's velocity (V_n) points in that direction. Neither the normal nor the tangential components (V_t) are drawn to scale. The inset detail of the hydrodynamic forces acting on a tail segment shows the acceleration reaction force acting in opposition to the quasi-steady normal force. The total force (shown in red) is the vector sum of these forces and the quasi-steady tangential force. (B,C) Representative forces and moments predicted for a single tail beat. Red arrows represent the total hydrodynamic force on individual tail segments; gray arrows show the direction of tail motion. For clarity, only the forces for the odd-numbered segments are drawn (segment length 0.11 mm). (B) In the first half of the tail beat, the tail moves to the right and experiences fluid forces opposing its motion. These forces generate moments in the clockwise direction with a time-averaged mean magnitude of -1.7×10^{-8} N m. (C) In the second half of the tail beat, the tail moves leftwards, and forces opposing this motion generate a mean counterclockwise moment of 2.3×10^{-8} N m. The time-averaged moment predicted for the entire tail beat is 0.3×10^{-8} N m, which will act to rotate the body in the counterclockwise direction. (D) The distribution of time-averaged moments generated by larvae (N=11) shows that all but one larva generated a counterclockwise-directed moment during swimming. The middle line in the box plot represents the median, the top and bottom edges of the box show the first quartile, error bars denote the second quartile and plus signs indicate values outside the second quartile.

moments perpendicular to that plane (Fig. 9A). Assuming a dorso-ventrally oriented tail fin, this means that kinematic asymmetries in lateral undulation can act only as a mechanism for generating a yawing moment.

To swim along a helix, a larva must generate pitching or rolling moments in addition to a yawing moment. These moments may be generated by the buoyancy force and the weight of the body (Fig. 9B). Buoyancy acts at the body's center of volume, and weight acts at its center of mass. If the body is composed of tissue of uniform density, the center of

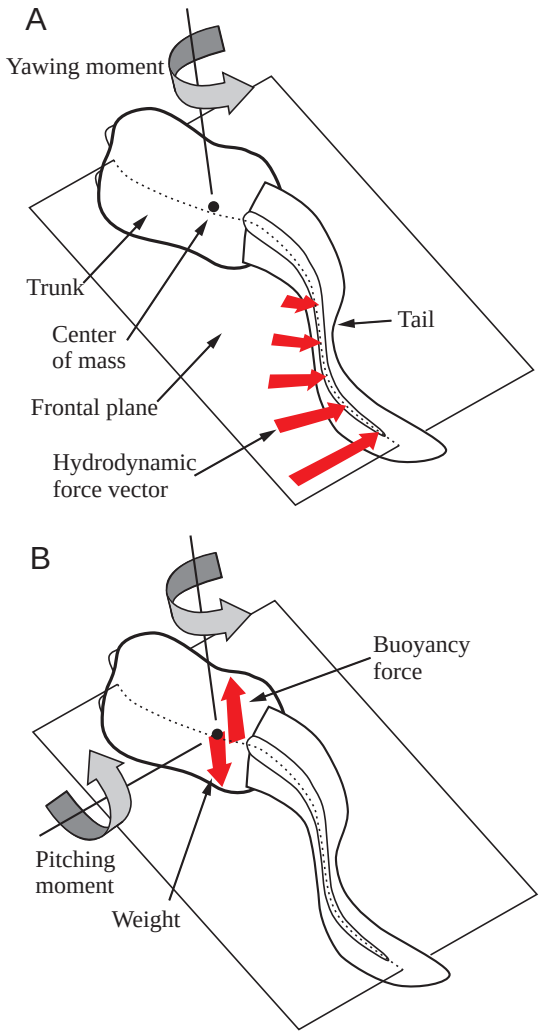

Fig. 9. The dynamics of swimming in ascidian larvae. A free-swimming larva is drawn from a dorsal and posterior perspective for an instant of time when the tail is beating towards the left. Some of the forces likely to influence the swimming mechanics are drawn to illustrate how moments acting on the center of mass could be generated in one (A) or two (B) dimensions. (A) Only hydrodynamic forces acting on the frontal plane of the body are drawn. As this larva swims forward, a yawing moment in the counterclockwise direction will tend to rotate the body in a counterclockwise direction around an axis perpendicular to the frontal plane. If only these hydrodynamic forces acted on the body for the entire tail beat, this larva would follow a circular trajectory lying on a plane coincident with the frontal plane of the body. (B) In addition to hydrodynamic forces, this larva has a buoyancy force and the weight of the body acting on it. The buoyancy force acting at the body's center of volume is posterior to the center of mass and therefore generates a pitching moment. With both pitching and yawing moments, the body would tend to rotate around an axis that is not perpendicular to the frontal plane. As a result, the larva would swim along a helical trajectory.

mass and center of volume would occur at the same point. Depending on the relative magnitudes of the body's buoyancy and weight, these forces will tend to accelerate the body down in the direction of gravity or up towards the water's surface. It is likely that combining the hydrodynamics of swimming with the weight and buoyancy of a body of uniform density could generate pitching or rolling moments. However, these moments would be greater if the body's tissues were not of uniform density. For example, if the anteriorly positioned otolith organ was more dense than the rest of the body, then the center of mass should be anterior to the center of volume. In this case, the distance between the center of mass and the center of buoyancy would create a moment arm that could generate a pitching moment, as shown in Fig. 9B. This 'non-uniform-density model' has been suggested to play a role in the geotaxic behavior of a variety of marine invertebrate larvae (Chia et al., 1984). This mechanism has been proposed for generating moments in the helical swimming of both bivalve larvae (Jonsson et al., 1991) and frog tadpoles (Roberts et al., 2000), but it remains to be integrated with hydrodynamic mechanisms in any system.

Table 1. *Swimming kinematics for 11 individuals of* Distaplia occidentalis

Individual	*L* (mm)	*U* (mm s^{-1})	*f* (Hz)	*Re*	κ_{CLmax} (rad mm^{-1})	κ_{CRmax} (rad mm^{-1})
1	3.34	29.1	14.7	92.9	1.7	0.9
2	3.39	22.0	17.2	71.3	2.0	1.4
3	3.35	25.3	15.1	80.9	1.6	0.9
4	3.58	22.6	11.6	77.3	1.7	1.1
5	3.37	23.4	18.5	75.3	2.0	1.0
6	3.49	31.0	20.0	103.3	2.4	1.3
7	3.96	28.6	21.7	108.3	1.3	0.9
8	3.56	40.7	16.6	138.4	2.2	0.9
9	3.54	28.1	18.5	95.0	2.0	0.8
10	3.60	29.5	25.0	101.6	2.5	0.7
11	3.33	24.4	20.0	77.4	1.6	1.0

L, body length; *U*, swimming speed; *f*, tail-beat frequency; *Re*, Reynolds number; κ_{CLmax}, maximum concave-left curvature; κ_{CRmax}, maximum concave-right curvature.

All values are expressed as the mean over the duration of the swimming sequence.

It is possible that the kinematic asymmetries described here could contribute to the generation of rolling or pitching moments if the tail fin were to twist while it undulates. Twisting along the longitudinal axis of the tail could occur if the notochord and muscle cells were not sufficiently stiff in torsion or if the dorsal half of the fin had a different flexibility from that of the ventral half. A twist in the tail fin could direct some of the hydrodynamic force out of the frontal plane of the body and, thereby, generate a moment arm for rolling or pitching rotation. Unfortunately, the video recordings for the present study did not have a spatial resolution great enough to observe twisting in the tail fin. However, in the few video frames in which the fin was visible, no twisting in the tail fin could be seen.

Helical versus *straight swimming*

Crenshaw (Crenshaw, 1993) suggested that organisms having single light-sensing organs with poor directional sensitivity may orient to light by swimming along a helical trajectory. This mechanism, known as helical klinotaxis, may facilitate phototaxis in ascidian larvae (Svane and Young, 1989), which have one ocellus. Alternatively, swimming along a straight trajectory requires the body to be stabilized against body rotation. This would probably be difficult for ascidian larvae because they possess no paired appendages for swimming and they are often found in turbulent environments (Berrill, 1950). Although helical swimming may not bestow ascidian larvae with greater speed, efficiency and maneuverability than straight swimming, it does appear to make oriented swimming possible despite a limited sensory and motor capacity. It seems plausible that high-performance larval swimming may be less important in the life history of an ascidian than sufficient phototaxis with a minimal morphological investment.

In summary, the results presented here suggest that swimming *D. occidentalis* larvae generate yawing moments by moving their tails asymmetrically (Fig. 8). Both the angle between the trunk and the tail (i.e. trunk angle; Fig. 1) and the tail curvature cause the tail to bend towards the left during swimming (Fig. 3, Fig. 4). This asymmetry is predicted by hydrodynamic theory to generate moments that should be great enough to rotate the body (Fig. 8) and therefore contribute to helical swimming. The flexural stiffness of the tail (Fig. 7) may be great enough that kinematic asymmetries are caused by the bent shape of the resting tail (Fig. 6).

List of symbols

A	surface area of a tail segment
C_n	normal force coefficient
C_t	tangential force coefficient
EI	flexural stiffness
f	tail-beat frequency
F	force
F_m	muscle force
$F_{reactive}$	reactive force on a tail segment
$F_{resistive}$	resistive force on a tail segment
F_{total}	total force on a tail segment
h	height of a tail segment
l	length of the tail in three-point bending
L	body length
m	added mass of a tail segment
n	tail segment number
$\hat{\mathbf{n}}$	unit vector normal to a tail segment's surface
Re	Reynolds number
s	position along length of body
s_i	position of inflection point on the body
S_m	cross-sectional area of muscle mass
t	time
$\hat{\mathbf{t}}$	unit vector tangential to a tail segment's surface
U	swimming speed
V_n	normal component of tail segment velocity
V_t	tangential component of tail segment velocity
z	distance from the tail midline to the center of muscle mass
α_{CL}	amplitude of concave-left curvature changes during swimming
α_{CR}	amplitude of concave-right curvature changes during swimming
α_θ	amplitude of trunk angle changes during swimming
β	baseline of periodic changes in trunk angle
ν	kinematic viscosity
δ	deflection of the tail
Δs	length of a tail segment
$\Delta\phi$	angular flexion between neighboring segments
ε	wave speed of inflection point propagation
θ	trunk angle
κ	curvature of a tail segment
$\overline{\kappa}$	mean curvature over the length of the tail
κ_{CL}	concave-left curvature
κ_{CLmax}	maximum concave-left curvature
κ_{CR}	concave-right curvature
κ_{CRmax}	maximum concave-right curvature
$\overline{\kappa_M}$	median tail curvature measured over a tail-beat cycle
ρ	water density
σ	muscle stress

I would like to thank M. Koehl for her guidance, H. Crenshaw for enlightening me about helical kinematics, E. Azizi for technical assistance, W. Getz for his comments on the manuscript and the Berkeley Biomechanics Group for general input. This research was supported with an NSF predoctoral fellowship and grants-in-aid of research from the Society for Integrative and Comparative Biology and Sigma Xi. Additional support came from National Science Foundation Grant OCE-9907120 to M. A. R. Koehl and the Office of Naval Research Grant N00014-98-0775 to M. A. R. Koehl.

References

Adams, D. S., Keller, R. and Koehl, M. A. R. (1990). The mechanics of notochord elongation, straightening and stiffening in the embryo of *Xenopus laevis*. *Development* **110**, 115–130.

Bergquist, P. R., Sinclair, M. E., Green, C. R. and Silyn-Roberts, H.

(1970). Adaptation to intertidal existence: reproductive cycles and larval behavior in Demospongiae. *Symp. Zool. Soc. Lond.* **25**, 247–271.
Berrill, N. J. (1950). *The Tunicata.* London: The Ray Society.
Boscov, J. S. and Feinleib, M. E. (1979). Phototactic response of *Chlamydomonas* to flashes of light. II. Response of individual cells. *Photochem. Photobiol.* **30**, 499–505.
Brokaw, C. J. (1965). Non-sinusoidal bending waves of sperm flagella. *J. Exp. Biol.* **43**, 155–169.
Burighel, P. and Cloney, R. A. (1997). Urochordata: Ascidiacea. In *Hemichordata, Chaetognatha and the Invertebrate Chordates*, vol. 15 (ed. F. W. Harrison), pp. 221–347. New York: John Wiley & Sons, Inc.
Cavey, M. J. and Cloney, R. A. (1972). Fine structure and differentiation of ascidian muscle. I. Differentiated caudal musculature of *Distaplia occidentalis* tadpoles. *J. Morph.* **138**, 349–374.
Chia, F. S., Buckland-Nicks, J. and Young, C. M. (1984). Locomotion of marine invertebrate larvae: a review. *Can. J. Zool.* **62**, 1205–1222.
Cloney, R. A. (1987). Phylum Urochordata, Class Ascidiacea. In *Reproduction and Development of Marine Invertebrates of the Northern Pacific Coast* (ed. M. F. Strathmann), pp. 607–646. Seattle: University of Washington Press.
Craig, J. J. (1989). *Introduction To Robotics: Mechanics and Control.* New York: Addison-Wesley.
Crenshaw, H. C. (1991). A technique for tracking spermatozoa in three dimensions without viscous wall effects. In *Comparative Spermatology, 20 Years After* (ed. B. Baccetti), pp. 353–357. New York: Raven Press.
Crenshaw, H. C. (1993). Orientation by helical motion. III. Microorganisms can orient to stimuli by changing the direction of their rotational velocity *Bull. Math. Biol.* **55**, 231–255.
Crenshaw, H. C., Ciampaglio, C. N. and McHenry, M. J. (2000). Analysis of the three-dimensional trajectories of organisms: estimates of velocity, curvature and torsion from positional information. *J. Exp. Biol.* **203**, 961–982.
Daniel, T. L. (1995). Invertebrate swimming: integrating internal and external mechanics. In *Symposia of the Society of Experimental Biology XLIX: Biological Fluid Dynamics* (ed. C. P. Ellington and T. J. Pedley), pp. 61–89. Cambridge: Company of Biologists Ltd.
Denny, M. W. (1988). *Biology and the Mechanics of the Wave-swept Environment.* Princeton: Princeton University Press.
Full, R. J. (1997). Invertebrate locomotor systems. In *The Handbook of Comparative Physiology* (ed. W. Dantzler), pp. 853–930. Oxford: Oxford University Press.
Grave, C. (1920). *Amaroucium pellucidum* (Leidy) form *constellatum* (Verrill). I. The activities and reactions of the tadpole larva. *J. Exp. Zool.* **30**, 239–257.
Grave, C. (1941). The 'eye-spot' and light-responses of the larva of *Cynthia partita. Biol. Bull.* **81**, 287.
Gray, J. (1933). Directional control of fish swimming. *Proc. R. Soc. Lond.* **113**, 115–125.
Gray, J. and Hancock, G. J. (1955). The propulsion of sea-urchin spermatozoa. *J. Exp. Biol.* **32**, 802–814.
Jeffery, W. R. (1997). Evolution of ascidian development. *Bioscience* **47**, 417–425.
Jennings, H. S. (1901). On the significance of the spiral swimming of organisms. *Am. Nat.* **35**, 369–378.
Jonsson, P. R., Andre, C. and Lindegarth, M. (1991). Swimming behavior of marine bivalve larvae in a flume boundary-layer flow: evidence for near-bottom confinement. *Mar. Ecol. Prog. Ser.* **79**, 67–76.
Jordan, C. E. (1992). A model of rapid-start swimming at intermediate Reynolds number: undulatory locomotion in the chaetognath *Sagitta elegans*. *J. Exp. Biol.* **163**, 119–137.
Katz, S. L. and Shadwick, R. E. (1998). Curvature of swimming fish midlines as an index of muscle strain suggests swimming muscle produces positive work. *J. Theor. Biol.* **193**, 243–256.
Knight-Jones, E. W. (1954). Relations between metachronism and the direction of ciliary beat in Metazoa. *Q. J. Microsc. Sci.* **95**, 503–521.
Lighthill, J. (1975). *Mathematical Biofluidynamics.* Philadelphia: Society for Industrial and Applied Mathematics.
Mast, S. O. (1921). Reactions to light in the larvae of the ascidians, *Amaroucium constellatum* and *Amaroucium pellucidum* with special reference to photic orientation. *J. Exp. Zool.* **34**, 149–187.
McHenry, M. J., Pell, C. A. and Long, J. H. (1995). Mechanical control of swimming speed: stiffness and axial wave form in undulating fish models. *J. Exp. Biol.* **198**, 2293–2305.
Miller, R. L. and Brokaw, C. J. (1970). Chemotactic turning behavior of *Tubularia* spermatozoa. *J. Exp. Biol.* **52**, 699–706.
Mladenov, P. V. and Chia, F. S. (1983). Speed of active movement of pelagic larvae of marine bottom invertebrates and their ability to regulate their vertical position. *Mar. Biol.* **23**, 11–17.
Roberts, A., Hill, N. A. and Hicks, R. (2000). Simple mechanisms organise orientation of escape swimming in embryos and hatchling tadpoles of *Xenopus laevis*. *J. Exp. Biol.* **203**, 1869–1885.
Russ, J. C. (1999). *The Image Processing Handbook.* Boca Raton, FL: CRC Press.
Sokal, R. R. and Rohlf, F. J. (1995). *Biometry*. New York: W. H. Freeman & Company.
Stokes, M. D. (1997). Larval locomotion of the lancelet *Branchiostoma floridae*. *J. Exp. Biol.* **200**, 1661–1680.
Svane, I. (1984). Observations on the long-term population dynamics of the perennial ascidian, *Ascidia mentula* on the Swedish west coast. *Biol. Bull.* **167**, 630–646.
Svane, I. and Young, C. M. (1989). The ecology and behavior of ascidian larvae *Oceanogr. Mar. Biol. Annu. Rev.* **27**, 45–90.
Thomas, G. B. and Finney, R. L. (1980). *Calculus and Analytic Geometry.* Reading, MA: Addison-Wesley Publishing Company.
Ullén, F., Deliagina, T. G., Orlovsky, G. N. and Grillner, S. (1995). Spatial orientation in the lamprey. I. Control of pitch and roll. *J. Exp. Biol.* **198**, 665–673.
Webb, P. W., Kostecki, P. T. and Stevens, E. D. (1984). The effect of size and swimming speed on locomotor kinematics of rainbow trout. *J. Exp. Biol.* **109**, 77–95.
Worcester, S. E. (1994). Adult rafting *versus* larval swimming: dispersal and recruitment of a botryllid ascidian on eelgrass. *Mar. Biol.* **121**, 309–317.
Young, C. M. (1995). Behavior and locomotion during the dispersal phase of larval life. In *Ecology of Marine Invertebrate Larvae* (ed. L. MacEdward), pp. 249–277. New York: CRC Press.